





Article

Spatial Contributions to ^1H NMR Chemical Shifts of Free-Base Porphyrinoids

Heike Fliegl ¹, Maria Dimitrova ², Raphael J. F. Berger ³ and Dage Sundholm ^{2,*}

¹ Institute of Nanotechnology, Karlsruhe Institute of Technology, Hermann-von-Helmholtz Platz 1, D-76344 Eggenstein-Leopoldshafen, Germany; heike.fliegl@kit.edu

² Department of Chemistry, University of Helsinki, A.I. Virtanens Plats 1, P.O. Box 55, FI-00014 Helsinki, Finland; maria.dimitrova@helsinki.fi

³ Chemistry of Materials, Paris-Lodron University of Salzburg, Jakob-Haringerstr. 2A, A-5020 Salzburg, Austria; raphael.berger@sbg.ac.at

* Correspondence: sundholm@chem.helsinki.fi

Abstract: A recently developed methodology for calculating, analyzing, and visualizing nuclear magnetic shielding densities is used for studying spatial contributions including ring-current contributions to ^1H nuclear magnetic resonance (NMR) chemical shifts of aromatic and anti-aromatic free-base porphyrinoids. Our approach allows a visual inspection of the spatial origin of the positive (shielding) and negative (deshielding) contributions to the nuclear magnetic shielding constants. Diatropic and paratropic current-density fluxes yield both shielding and deshielding contributions implying that not merely the tropicity of the current density determines whether the contribution has a shielding or deshielding character. Instead the shielding or deshielding contribution is determined by the direction of the current-density flux with respect to the studied nucleus.

Keywords: magnetically induced current densities; London orbitals; gauge-including atomic orbitals; nuclear magnetic shielding constants



Citation: Fliegl, H.; Dimitrova, M.; Berger R.J.F.; Sundholm, D. Spatial Contributions to ^1H NMR Chemical Shifts of Free-Base Porphyrinoids. *Chemistry* **2021**, *3*, 1005–1021. <https://doi.org/10.3390/chemistry3030072>

Academic Editors: Andrea Peluso and Guglielmo Monaco

Received: 15 August 2021

Accepted: 1 September 2021

Published: 5 September 2021

Publisher's Note: MDPI stays neutral with regard to jurisdictional claims in published maps and institutional affiliations.



Copyright: © 2021 by the authors. Licensee MDPI, Basel, Switzerland. This article is an open access article distributed under the terms and conditions of the Creative Commons Attribution (CC BY) license (<https://creativecommons.org/licenses/by/4.0/>).

1. Introduction

This article is dedicated to Professor Riccardo Zanasi on the occasion of his 70th birthday. He graduated from the University of Modena, Italy in 1975, studying electric and magnetic properties of molecules. He is one of the pioneers in the field of current-density calculations with his first article from 1981 on the ring-current model of the cyclopropenyl cation [1]. The “continuous transformation of the origin of the current density (CTOCD) method” from 1994 [2], which Keith and Bader called “continuous set of gauge transformations (CSGT)”, was the starting point for the SYSMO and SYSMOIC program packages [3,4]. Professor Zanasi has published about 70 scientific articles on computational studies of magnetically induced current densities in molecules with “current density” in the title. He is the main developer of the SYSMO code. The topic of this article is closely related to the research interests of Professor Zanasi, since we have calculated and analyzed magnetic shielding densities (MSD) of free-base porphyrinoids. MSD is the spatial contribution to the chemical shifts in nuclear magnetic resonance (NMR) spectroscopy and calculated using the magnetically induced current density (Figure S1).

For the aromatic benzene molecule, it is well known that the magnetically induced ring current leads to a downfield shift of the ^1H NMR signal, because the diatropic ring current induces a secondary magnetic field with field lines forming closed loops around the ring current. The field lines point in the opposite direction to the applied magnetic field inside the ring, while outside the ring they are parallel to the external field, see Figure 1. The hydrogen atoms of benzene outside the ring-current pathway are deshielded because the induced magnetic field enhances the applied one. However, a recent study of the MSD of benzene showed that the ring current leads to regions with significant shielding and

deshielding contributions [5]. The ring-current contribution to the ^1H NMR chemical shift of benzene can be estimated to be about 1.7 ppm from the experimental chemical shifts of benzene (5.6 ppm) and the vinylic hydrogen atoms of cyclohexene (7.3 ppm).

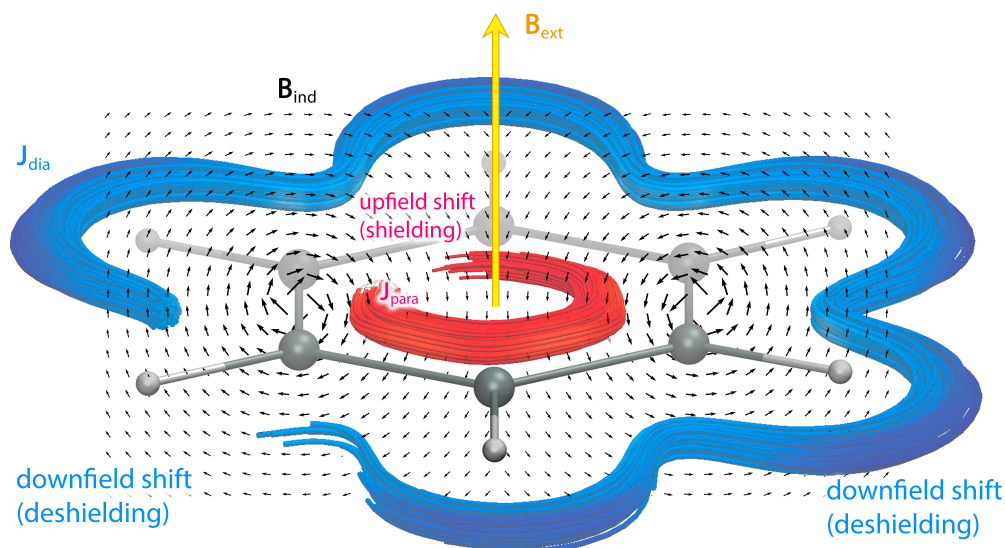


Figure 1. Illustration of the induced magnetic field (black arrows) when the aromatic benzene is exposed to an external magnetic field (yellow) perpendicular to the molecular ring. The magnetically induced current density circling in the classical direction is called diatropic (blue) and the one flowing in the opposite direction is paratropic (red). The induced magnetic field in the center of the ring points in the opposite direction relative to the applied field, while it deshields the nuclear magnetic moment of the hydrogen atoms outside the ring.

The origin of the ^1H NMR chemical shifts is even more complex when studying aromatic or anti-aromatic molecules bearing hydrogen atoms inside the ring-current pathway. The aromatic free-base *trans*-porphyrin is an example of such molecules. The accepted notion is that the ^1H NMR signal of the inner hydrogen is upfield shifted and the ^1H NMR signals of the *meso* and β hydrogen nuclei are downfield shifted because the direction of the induced magnetic field is in the opposite direction to the applied one inside the porphyrin ring and parallel to the external field outside the ring. The chemical shifts of the ^1H NMR signals of anti-aromatic molecules are influenced in the opposite manner compared to aromatic ones because anti-aromatic molecules sustain strong paratropic ring currents. Measurements of the ^1H NMR chemical shifts of the inner or outer hydrogen atoms of porphyrinoids are often used for assessing their aromatic character experimentally. Calculated ^1H NMR chemical shifts can be used for estimating the direction and the strength of the magnetically induced ring current and for identifying porphyrinoid tautomers [6–8].

The ring-current model of aromatic and anti-aromatic molecules [9,10] with a current-density pathway forming a closed loop in the π orbitals above and below the molecular ring might be a somewhat oversimplified explanation of the aromatic or anti-aromatic contribution to the ^1H NMR chemical shifts. Since the vector potential of the nuclear magnetic moment declines rapidly with the distance from the nucleus, the largest contributions to the ^1H NMR chemical shifts originate from the current density near the considered nucleus.

Instead of the well known nucleus-independent-chemical-shift (NICS) functions [11–13], we investigate the MSD calculated using the magnetically induced current density. The MSD yields detailed information about spatial contributions to the NMR chemical shifts. The MSD calculated using the Biot–Savart expression for NMR chemical shifts can be more useful for interpreting experimental NMR data than alternative approaches [14], since it is possible not only to quantify the amount of positive and negative

contributions to the shielding constant of a specific nucleus but also to identify the spatial origin of the most relevant contributions.

In this work, we apply our methodology for analyzing spatial contributions to the ^1H NMR magnetic shieldings of inner and outer hydrogen atoms of free-base *trans*-porphyrin, free-base *trans*-isophlorin, and free-base *trans*-norcorrole (Figures S2 and S3). Free-base *trans*-porphyrin serves as the typical aromatic porphyrin. Free-base *trans*-isophlorin proposed by Woodward represents anti-aromatic porphyrins [15,16], whereas anti-aromatic norcorroles are the smallest tetrapyrrole porphyrinoids that have been synthesized [17–19]. The underlying theory is briefly described in Section 2. The computational levels are presented in Section 3.1 and the employed numerical methods for calculating the shielding density are described in Section 3.2. The obtained shielding densities are discussed in Section 4. Finally, the study is summarized and concluded in Section 5.

2. Theory

Nuclear magnetic shieldings are usually calculated using the gradient theory of electronic structure calculations as the mixed second derivative of the electronic energy with respect to the strength of the external magnetic field and the size of the nuclear magnetic moment [20–24]. The components of the nuclear magnetic shielding tensor, σ , in the α and β Cartesian directions can also be calculated as the second derivative of the magnetic interaction energy expressed as a spatial integral over the scalar product of the magnetically induced current-density susceptibility ($\partial\mathbf{J}^{\mathbf{B}}(\mathbf{r})/\partial B_{\beta}$) due to the external magnetic field (\mathbf{B}) and the first derivative of the vector potential of the nuclear magnetic moment (\mathbf{m}_I) with respect to the size of the nuclear magnetic moment ($\partial\mathbf{A}^{\mathbf{m}_I}(\mathbf{r})/\partial m_{I\alpha}$) calculated at vanishing \mathbf{B} and \mathbf{m}_I [14,25–27],

$$\sigma_{\alpha\beta} = - \int \frac{\partial\mathbf{J}^{\mathbf{B}}(\mathbf{r})}{\partial B_{\beta}} \cdot \frac{\partial\mathbf{A}^{\mathbf{m}_I}(\mathbf{r})}{\partial m_{I\alpha}} \, d\mathbf{r} \Bigg|_{\substack{\mathbf{B}=\mathbf{0} \\ \mathbf{m}_I=\mathbf{0}}} \quad (1)$$

The vector potential $\mathbf{A}^{\mathbf{m}_I}(\mathbf{r})$ of the nuclear magnetic dipole moment in international system of units (SI) is given by

$$\mathbf{A}^{\mathbf{m}_I}(\mathbf{r}) = \frac{\mu_0}{4\pi} \mathbf{m}_I \times \frac{\mathbf{r} - \mathbf{R}_I}{|\mathbf{r} - \mathbf{R}_I|^3}, \quad (2)$$

where \mathbf{R}_I is the position of nucleus I and μ_0 is the vacuum permeability [28]. This scheme is implemented in the gauge-including magnetically induced currents (GIMIC) method [29–34] for calculating the current-density susceptibility tensor (CDT) [35,36] as described in Section 3.2. Similarly, the nuclear magnetic shielding tensor can be calculated from the current density induced by the nuclear magnetic moment multiplied with the vector potential of the external magnetic field [14,36–38]. This approach has been employed in other studies [39,40], however it has not been considered in this work.

Even though the NMR shieldings obtained with the gradient theory and the integration approaches are the same, the integration method can provide information about orbital and spatial contributions to a given NMR chemical shift [36,37,41]. When a numerical representation of the current density is gauge-origin independent, the calculated NMR chemical shifts obtained with the integration approach are also independent of the gauge origin. We use the GIMIC method [29–32] for calculating current densities, however, the CTOD approach also leads to gauge-origin independence [2,4,42–44]. The spatial distribution of the shielding density provides detailed information about the origin of the individual elements of the nuclear magnetic shielding tensor, as well as the shielding constants [5,44–50]. Dividing the magnetic shielding density into positive and negative parts yields the spatial origins of the shielding and deshielding contributions to the shielding tensor and the isotropic shielding constants, providing a rigorous physical basis for interpreting NMR chemical shifts.

3. Computational Methods

3.1. Electronic and Molecular Structure Calculations

The molecular structures of free-base *trans*-porphyrin, free-base isophlorin, free-base *trans*-norcorrole were optimized with Turbomole [51] version 7.5 employing the B3LYP density functional [52–54], the def2-TZVP basis set using the resolution of the identity (RI) approximation [55,56], and the m5 quadrature grid [57]. The molecular structure of isophlorin was assumed to be planar. The planar isophlorin structure is not a minimum on the potential energy surface but a saddle point with several imaginary vibrational frequencies due to out-of-plane motions of the inner hydrogens. The optimized molecular structures are shown in Figure 2 and the Cartesian coordinates are given in the electronic supporting information (ESI). The NMR shielding constants were calculated with Turbomole at the BHandHLYP (LIBXC ID 436) [53,58,59] level of theory using gauge-including atomic orbitals (GIAO) [20,60–62]. The BHandHLYP functional that has 50% Hartree–Fock exchange yielded accurate magnetizabilities in a recent benchmark study [41]. For all NMR calculations the pcseg-3 basis set has been employed which has been optimized for the calculation of NMR parameters [63]. The pcseg-3 basis sets have been obtained from the EMSL basis set exchange library [64–66]. For the visualizations, the smaller def2-TZVP basis set has been employed which was tested to be sufficient.

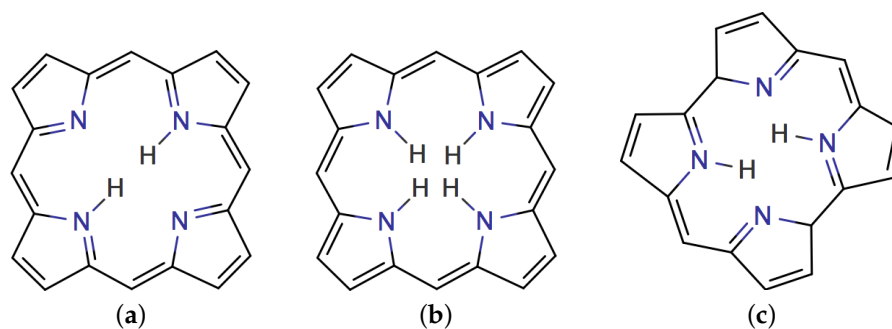


Figure 2. The molecular structure of (a) free-base *trans*-porphyrin, (b) free-base isophlorin, and (c) free-base *trans*-norcorrole.

3.2. Magnetic Shielding-Density Calculations

The use of finite one-particle basis sets in the calculation of CDT introduces a gauge dependence even though the exact solution of the Schrödinger equation is gauge invariant. However, the calculated CDT can be made gauge-origin independent by using GIAOs. GIAOs also lead to a fast basis-set convergence of the current density and magnetic properties, because GIAOs are correct to first order in the magnetic response for any choice of the gauge origin, whereas ordinary basis functions are correct only to zeroth order [67]. The GIAOs are given by [20,60]

$$\chi_{\mu}(\mathbf{r}) = e^{-i(\mathbf{B} \times [\mathbf{R}_{\mu} - \mathbf{R}_0] \cdot \mathbf{r})/2} \chi_{\mu}^{(0)}(\mathbf{r}), \quad (3)$$

where i is the imaginary unit and $\chi_{\mu}^{(0)}(\mathbf{r})$ is a standard Gaussian-type basis function centered at \mathbf{R}_{μ} . The gauge origin is eliminated from the CDT expression when using GIAOs [29,31,32]. The CDT expression of the GIMIC method is

$$\frac{\partial \mathbf{J}_{\alpha}^{\mathbf{B}}(\mathbf{r})}{\partial B_{\beta}} = \sum_{\mu\nu} D_{\mu\nu} \left[\frac{\partial \chi_{\mu}^{*}(\mathbf{r})}{\partial B_{\beta}} \frac{\partial \tilde{h}(\mathbf{r})}{\partial m_{I_{\alpha}}} \chi_{\nu}(\mathbf{r}) + \chi_{\mu}^{*}(\mathbf{r}) \frac{\partial \tilde{h}(\mathbf{r})}{\partial m_{I_{\alpha}}} \frac{\partial \chi_{\nu}(\mathbf{r})}{\partial B_{\beta}} - \sum_{\gamma} \epsilon_{\alpha\beta\gamma} \chi_{\mu}^{*}(\mathbf{r}) \frac{\partial^2 \tilde{h}(\mathbf{r})}{\partial m_{I_{\alpha}} \partial B_{\gamma}} \chi_{\nu}(\mathbf{r}) \right] + \sum_{\mu\nu} \frac{\partial D_{\mu\nu}}{\partial B_{\beta}} \chi_{\mu}^{*}(\mathbf{r}) \frac{\partial \tilde{h}(\mathbf{r})}{\partial m_{I_{\alpha}}} \chi_{\nu}(\mathbf{r}), \quad (4)$$

where \mathbf{D} is the density matrix and $\partial \mathbf{D} / \partial \mathbf{B}$ are the magnetically perturbed density matrices in the atomic-orbital basis, $\epsilon_{\alpha\beta\gamma}$ is the Levi–Civita symbol with $\alpha, \beta, \gamma \in \{x, y, z\}$. $\tilde{h}(\mathbf{r})$

denotes that the singular $|\mathbf{r} - \mathbf{R}_I|^{-3}$ denominator appearing in all terms is omitted. The non-singular magnetic interaction operators are

$$\frac{\partial \tilde{h}(\mathbf{r})}{\partial \mathbf{m}_I} = (\mathbf{r} - \mathbf{R}_I) \times \mathbf{p} \quad (5)$$

and

$$\frac{\partial^2 \tilde{h}(\mathbf{r})}{\partial \mathbf{m}_I \partial \mathbf{B}} = \frac{1}{2} [(\mathbf{r} - \mathbf{R}_O) \cdot (\mathbf{r} - \mathbf{R}_I) \mathbf{1} - (\mathbf{r} - \mathbf{R}_O)(\mathbf{r} - \mathbf{R}_I)], \quad (6)$$

where \mathbf{R}_I is the position of nucleus I . All terms containing the gauge origin \mathbf{R}_O cancel in Equation (4), making the CDT and the Biot–Savart expression independent of the gauge origin. All nuclear-position terms in Equation (4) also cancel, eliminating the coordinates of the nucleus I from the CDT expression. The current density depends implicitly on the nuclear positions, since the basis functions are located at the nuclei.

The Biot–Savart expression for the nuclear magnetic shielding tensor of nucleus I , $\sigma_{\alpha\beta}^I$, is then

$$\sigma_{\alpha\beta}^I = -\frac{\mu_0}{4\pi} \sum_{\gamma\delta} \epsilon_{\alpha\delta\gamma} \int \frac{(r_\delta - R_{I\delta})}{|\mathbf{r} - \mathbf{R}_I|^3} \frac{\partial J_\gamma^{\mathbf{B}}(\mathbf{r})}{\partial B_\beta} d\mathbf{r}, \quad (7)$$

where μ_0 is the vacuum permeability and $\alpha, \beta, \gamma, \delta \in \{x, y, z\}$. The integrand in Equation (7) is the magnetic shielding density (MSD) containing spatial contributions to the nuclear magnetic shielding of nucleus I [5,14,25,26,44,46,48–50]. Visualization of the MSD yields information about the spatial origin of the NMR chemical shift of nucleus I . NMR chemical shifts can be interpreted by plotting the positive and negative parts of the integrand separately. The visualization provides information about shielding and deshielding contributions originating from the relative direction of the current density with respect to the investigated atom I [5,32,68]. Contributions to NMR shieldings can be calculated by integrating the Biot–Savart expression in Equation (7) numerically using the CDT calculated in the integration points. We have implemented a numerical integration scheme into the GIMIC program for calculating spatial contributions to nuclear magnetic shieldings and magnetizabilities [5,34,41]. Atomic contributions can be obtained by integrating atomic domains generated by the NUMGRID library [69] using Becke’s multicenter scheme [70]. The atomic domains are constructed using the Becke partitioning scheme with the iteration order $k = 3$ in the construction of the cut-off function [70]. Angular integration of the atom-centered domains is performed with Lebedev’s angular grid [71] and the radial integration grid is constructed as suggested by Lindh et al. [72]. The density matrix, the magnetically perturbed density matrices and the basis-set data are obtained from Turbomole [51] calculations of NMR shielding constants.

4. Results and Discussion

4.1. Free-Base *trans*-Porphyrin

We have analyzed the ring-current contribution to the ^1H NMR shielding constants by plotting the spatial distribution of its isotropic shielding constant (σ_{iso}). The ^1H NMR shielding density of *trans*-porphyrin in Figure 3 shows that the inner hydrogen atoms have shielding contributions in the molecular plane from the ring current along the outer edge of the molecule [73]. However, a stronger shielding contribution originates from the innermost pathway via the four pyrrole nitrogen atoms. The largest shielding contribution appears near the studied hydrogen, because of the singular denominator of the vector potential of the magnetic moment of the inner hydrogen. The nitrogen atom also sustains a local diatropic current-density vortex extending around the N–H bond. The paratropic ring current inside the porphyrin ring and the diatropic current-density vortex of the nitrogen of the adjacent pyrrole rings cause deshielding. A deshielding area is also seen at the other inner hydrogen where the paratropic ring-current flux inside the porphyrin ring is closest to the studied inner hydrogen. The MSD of σ_{iso} of the inner hydrogen is seen 1 Å above the molecular plane in Figure 3. The effect of the ring current is weaker there than in the

molecular plane. The deshielding contributions are also very small at a distance of 1 Å from the molecular plane because the paratropic ring current vanishes there.

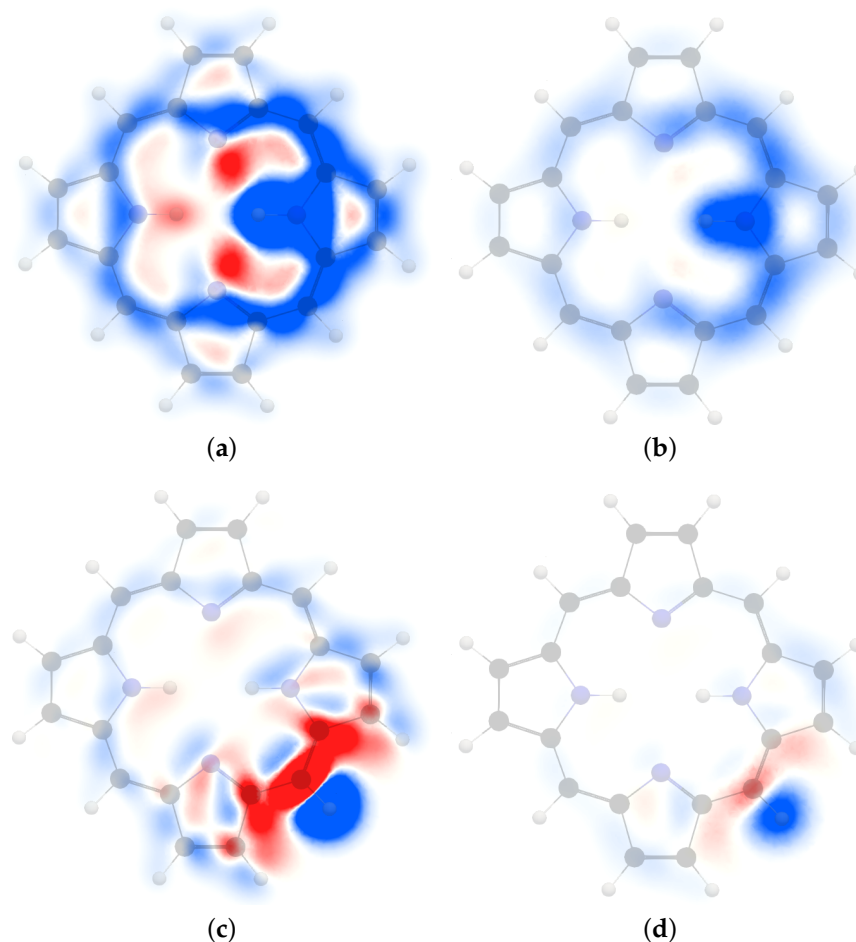


Figure 3. The isotropic ¹H NMR shielding density of the inner hydrogen of *trans*-porphyrin in (a) the molecular plane and (b) 1 Å above the plane. The ¹H NMR shielding density of the *meso* hydrogen in (c) the molecular plane and (d) 1 Å above the *trans*-porphyrin plane. The shielding contributions are shown in blue and the deshielding contributions in red. The employed range is [−0.2, 0.2].

The MSD of the *meso* hydrogen in the molecular plane shown in Figure 3 reveal a strong shielding contribution near the hydrogen. A deshielding contribution caused by the diatropic ring current flux in the vicinity of the *ipso* carbon and the nearest α carbon atoms of the adjacent pyrrole rings. The more distant part of the diatropic ring current shields the nucleus of the *meso* hydrogen. The paratropic ring current inside the porphyrin results in a shielding contribution inside the *meso* carbon. One can also see alternating shielding and deshielding contributions from the paratropic ring current inside the porphyrin ring due to its relative direction with respect to the nucleus of the studied *meso* hydrogen. The MSD of the *meso* hydrogen 1 Å above the molecular plane shown in Figure 3 has a similar pattern as in the molecular plane. However, the contributions away from the molecular plane are much smaller.

The 3D picture of the MSD of the inner hydrogen in Figure 4 shows the shielding contribution from the diatropic ring current along the outer edge of the molecule and the deshielding contribution from the paratropic ring current inside the porphyrin ring. Lots of atoms contribute significantly to the isotropic shielding constant of the inner hydrogen of 37.52 ppm, because the distances from it to many of the other atoms are relatively short. The local contribution from the inner H is only 12.85 ppm. The contributions from N_{ipso} , C_α of the same pyrrole ring, the nearest C_{meso} , and the nearest C_α atoms of the adjacent pyrrole

rings are 5.28, 2.35, 1.53, and 1.16 ppm, respectively. The rest of the atomic contributions to σ_{iso} of the inner hydrogen is in the range of ± 1 ppm. Contributions from each atom to the σ_{iso} of the hydrogen atoms are reported in the ESI and summarized in Figure 5. The 3D pictures of the MSD of the *meso* and β hydrogen atoms are reported in the ESI.

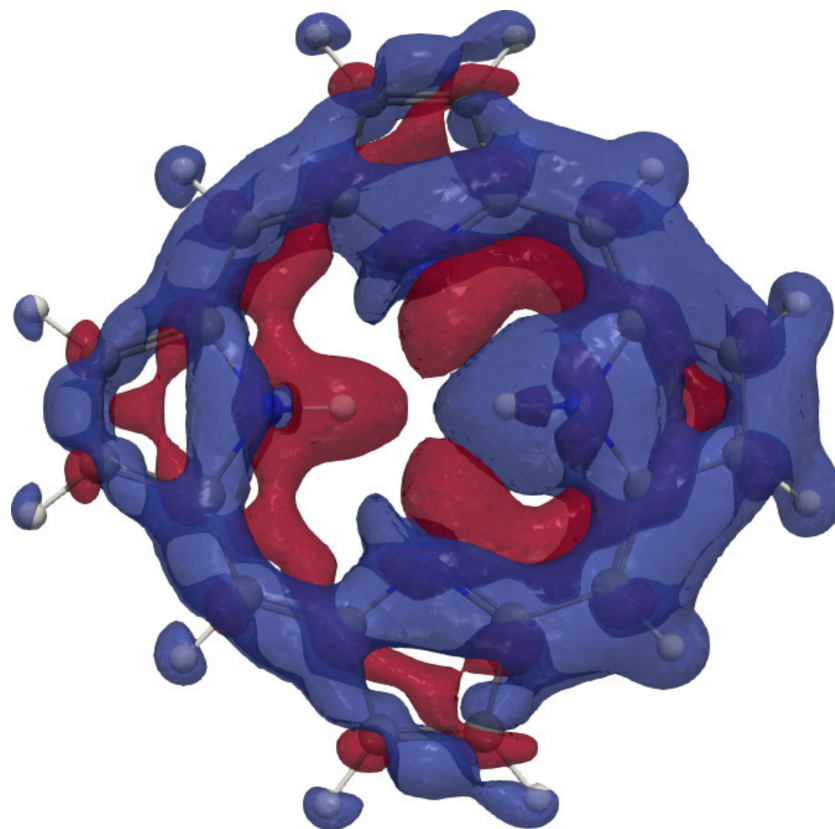


Figure 4. The isotropic ^1H NMR shielding density of the inner hydrogen of *trans*-porphyrin. The shielding contributions are shown in blue and the deshielding contributions in red. An isovalue of ± 0.04 has been used.

4.2. Free-Base Isophlorin

The spatial distribution of the isotropic MSD of free-base isophlorin in Figure 6 shows that the inner hydrogen atoms and the *meso* hydrogen atoms have deshielding contributions from the paratropic ring current in the molecular plane along the outer edge of the molecule. The shielding contributions originate mainly from the current density in the vicinity of the studied inner hydrogen.

The 3D contour of the ring-current contribution to σ_{iso} of the inner hydrogen is shown in Figure 7. The ring current following the inner route is stronger than the one via the β carbons which means that its contribution to the shielding density is bigger. Furthermore, the vector potential of the nuclear magnetic moment, $\mathbf{A}^{\text{ml}}(\mathbf{r})$ declines rapidly with increasing distance from the nucleus I .

Dividing the MSD of the inner hydrogen into atomic domains that are integrated separately shows that many atoms contribute significantly to its σ_{iso} value of -6.28 ppm. Since the distances from the inner hydrogen to adjacent atoms are short, the vector potential of the nuclear magnetic moment of the inner hydrogen has a significant amplitude at the atomic domains of the neighboring atoms leading to large atomic contributions to σ_{iso} of the inner hydrogen.

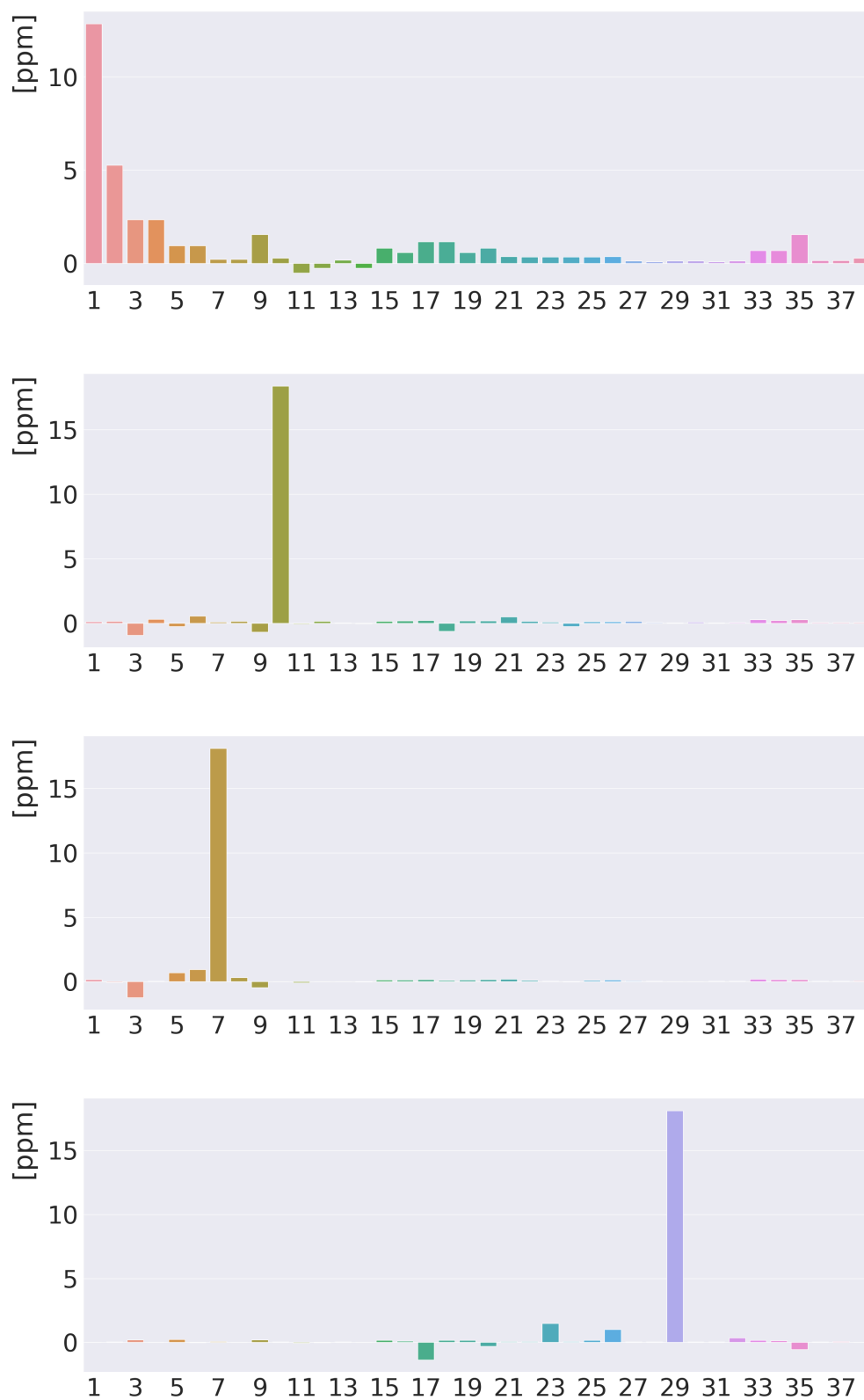


Figure 5. Atomic contributions (in ppm) to the isotropic ^1H NMR shielding constants of free-base *trans*-porphyrin. From above: the inner hydrogen, the *meso* hydrogen, the β hydrogen atoms of the pyrrole ring with an inner hydrogen, and the β hydrogen atoms of the pyrrole ring without an inner hydrogen. The atoms are numbered along the x axis in the same order as in the ESI.

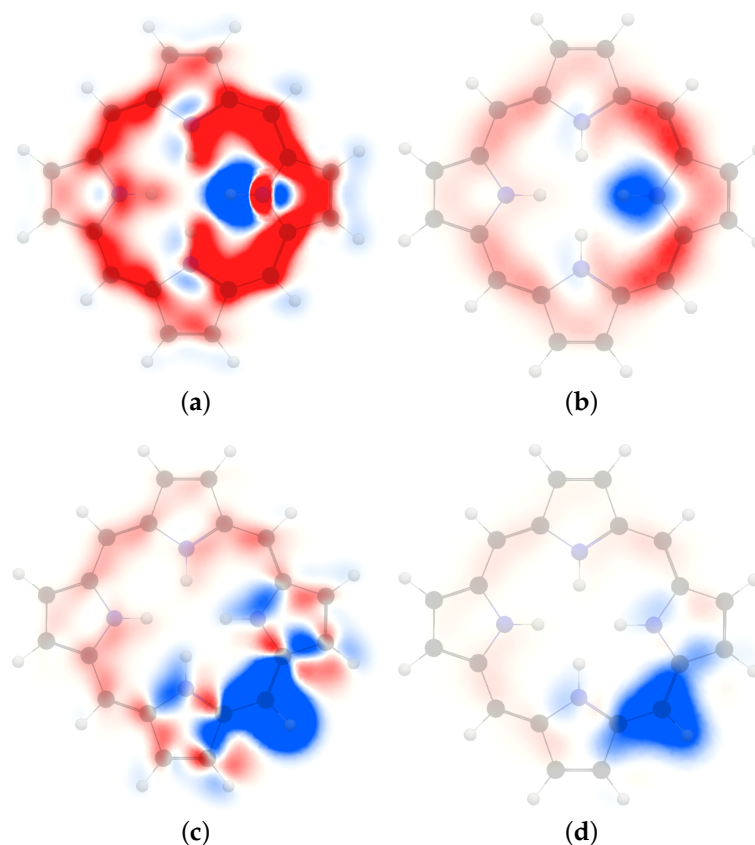


Figure 6. The isotropic ^1H NMR shielding density of the inner hydrogen of free-base isophlorin in (a) the molecular plane and (b) 1 Å above the plane. The ^1H NMR shielding density of the *meso* hydrogen in (c) the molecular plane and (d) 1 Å above the free-base isophlorin plane. The shielding contributions are shown in blue and the deshielding contributions in red. The employed range is $[-0.2, 0.2]$.

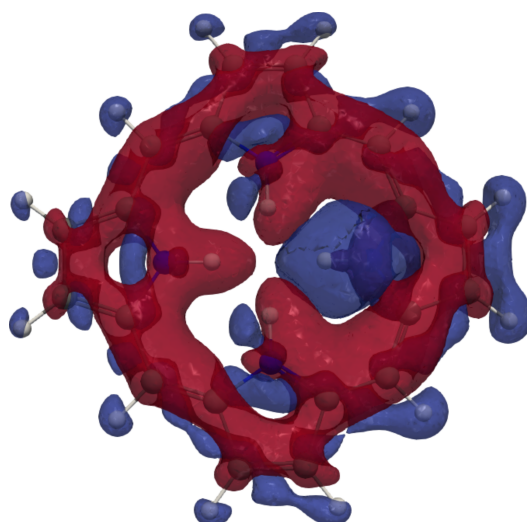


Figure 7. The isotropic ^1H NMR shielding density of the inner hydrogen of free-base isophlorin. The shielding contributions are shown in blue and the deshielding contributions in red. An isovalue of ± 0.04 has been used. The corresponding pictures of the ^1H NMR shielding densities of the β hydrogen atoms are given in the ESI.

The local contribution from the atomic domain of the inner hydrogen is 16.46 ppm, whereas contributions from adjacent atoms are negative. The contributions from the

adjacent and *trans* inner hydrogen atoms are -0.79 ppm and -0.57 ppm, respectively. The contributions from N_{ipso} , C_{α} of the same pyrrole ring, the nearest C_{meso} , and the C_{α} atoms of the neighboring pyrrole ring are 0.96 , -2.18 , -2.38 , and -1.85 ppm, respectively. The rest of the atomic contributions are in the range of ± 1 ppm. Contributions from each atom to the σ_{iso} of the inner hydrogen are summarized in Figure 8 and the atomic contributions from all atoms to σ_{iso} of the inner hydrogen are reported in the ESI.



Figure 8. Atomic contributions (in ppm) to the isotropic ^1H NMR shielding constants of free-base isophlorin. From above: the inner hydrogen, the *meso* hydrogen, the β hydrogen atoms of the pyrrole ring. The atoms are numbered along the x axis in the same order as in ESI.

The paratropic ring current along the outer edge of the molecule in the molecular plane causes deshielding of the *meso* hydrogen, which has also shielding and deshielding contributions along the inner ring-current pathway at the adjacent pyrrole rings due to the relative direction of the ring current with respect to the studied nucleus. The MSD of the *meso* hydrogen in Figure 6 has shielding contributions near the hydrogen and the *ipso* carbon originating from the paratropic ring current inside the hydrogen and from the diatropic current-density flux outside the hydrogen. The MSD contributions at the

molecular plane and 1 Å away from it has a similar shape but is weaker as the distance from the molecular plane increases.

Calculations of the atomic contributions to the MSD show that the shielding domain of the *meso* hydrogen atoms includes the nearest α carbons. Since the distances from the *meso* hydrogen to other atoms are longer than for the inner hydrogen, the contributions from the adjacent atoms are somewhat smaller than for the α carbons.

The largest atomic contributions to σ_{iso} of the *meso* hydrogen are 18.80, 12.40, 2.70, and 1.66 ppm from the *meso* hydrogen, C_{meso} , and from the two closest C_{α} atoms. The largest atomic contributions to σ_{iso} of the β hydrogen are 18.48, 7.06, 2.94, and 1.23 ppm from the studied β hydrogen, C_{ipso} , the adjacent C_{β} and C_{meso} , respectively. Contributions from each atom to the σ_{iso} of the hydrogen atoms are summarized in Figure 8. The atomic contributions to σ_{iso} of the *meso* and β hydrogen atoms from all atoms are reported in the ESI. The 3D pictures of the MSD of the *meso* and β hydrogen atoms are reported in the ESI.

4.3. Free-Base *trans*-Norcorrole

The MSD of the inner hydrogen of free-base *trans*-norcorrole in Figure 9 is dominated by deshielding contributions around the outer edge of the molecule that originate from the strong paratropic ring current [74–76]. The ring-current contribution is strong in the molecular plane as well as in a plane 1 Å away from it, where the deshielding contributions completely dominate. Diatropic contributions appear in the molecular plane between the α carbons and the nitrogen atoms inside the pyrrole rings due to the local diatropic current-density flux around the nitrogen moiety, which leads to a large shielding domain near the studied inner hydrogen that extends to the plane 1 Å away from the molecular plane.

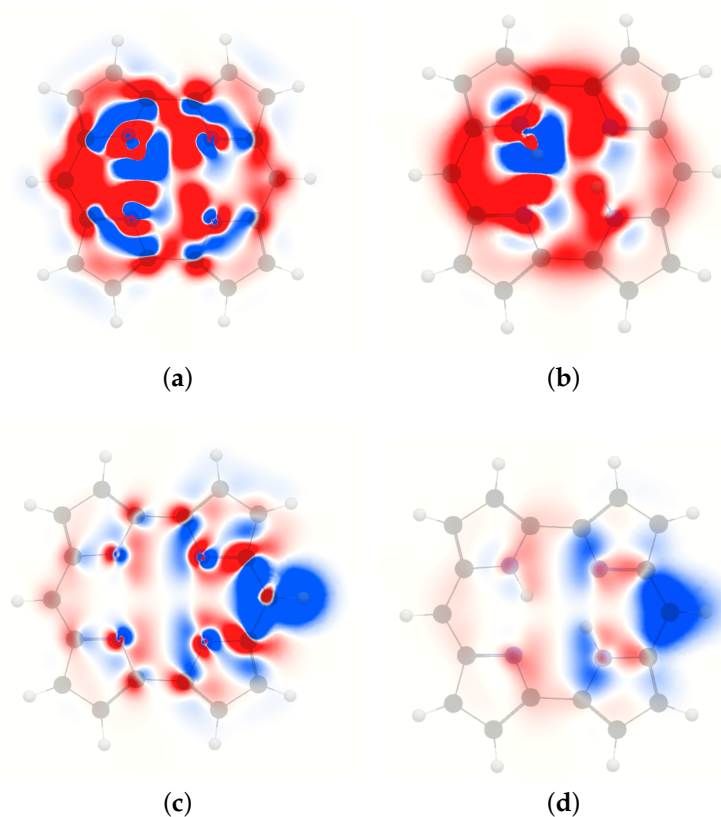


Figure 9. The isotropic ^1H NMR shielding density of the inner hydrogen of *trans*-norcorrole in (a) the molecular plane and (b) 1 Å above the plane. The ^1H NMR shielding density of the *meso* hydrogen in (c) the molecular plane and (d) 1 Å above the *trans*-norcorrole plane. The shielding contributions are shown in blue and the deshielding contributions in red. The employed range is $[-0.2, 0.2]$.

The 3D contour of the MSD of the inner hydrogen in Figure 10 shows a completely dominating deshielding contribution originating from the paratropic ring current. The diatropic ring current along the outer perimeter of free-base *trans*-norcorrole results in shielding contributions that are larger in the vicinity of the inner hydrogen than on the remote side of the molecule because the magnetic vector potential declines rapidly at longer distances. The significant shielding domain appears near the studied inner hydrogen.

Calculations of MSD contributions from atomic domains show that many atoms contribute to σ_{iso} of the inner hydrogen due to the short distances between it and the atoms inside norcorrole. The atomic contribution of 10.28 ppm from the studied inner hydrogen is shielding, whereas the atomic contributions from atoms in the vicinity are deshielding. The contributions from the C_{α} atoms are in the range of -1.09 to -1.99 ppm. The contribution from the nearest *meso* carbon is -2.04 ppm. The contributions from the adjacent and *trans* nitrogen atoms are -2.19 and -1.01 ppm, respectively. The contribution from the *ipso* nitrogen is only -0.78 ppm. The small negative contributions from many atoms leads to a negative σ_{iso} of -8.73 ppm even though the local contribution is of about the same size but positive.

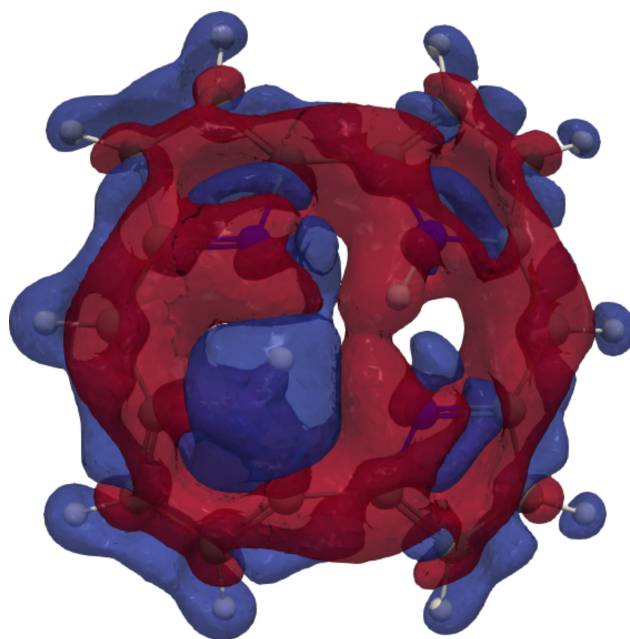


Figure 10. The isotropic ^1H NMR shielding density of the inner hydrogen of *trans*-norcorrole. The shielding contributions are shown in blue and the deshielding contributions in red. An isovalue of ± 0.04 has been used. The corresponding pictures of the ^1H NMR shielding densities of the *meso* and β hydrogen atoms are given in the ESI.

The MSD of the *meso* hydrogen consists of alternating shielding and deshielding contributions in the molecular plane, as well as in the plane 1 \AA away from it. The main shielding areas appear in the vicinity of the studied *meso* hydrogen originating from the paratropic ring current inside it and the diatropic current density outside the *meso* hydrogen. The current density around the nitrogen moieties leads to alternating shielding and deshielding contributions, whereas the typical ring-current contributions from other parts of the molecule are not very pronounced. The main atomic contributions to the *meso* hydrogen are 18.56, 8.93, and 1.06 ppm from the *meso* hydrogen, C_{ipso} and one of the nearest C_{α} atoms, respectively. The atomic shielding contributions are localized to the nearest atoms because other atoms are very far away from the *meso* hydrogen, implying that the amplitude of the vector potential of its nuclear magnetic moment vanishes at atoms on the other side of the porphyrinoid ring.

The magnetic shieldings of the β hydrogen atoms are in the range of 26.89 to 28.16 ppm. Since the differences are small, we only discuss one type of β hydrogen atoms. The σ_{iso}

value of atom 21, which is one of the β hydrogen atoms of a pyrrole ring without an inner hydrogen, has a local contribution of 18.24 ppm. The largest atomic contributions from adjacent atoms are 3.73, 2.23, 1.25, and 1.16 ppm from C_{ipso} , nearest C_{α} , nearest C_{β} that is not C_{ipso} and the nitrogen of the same pyrrole ring, respectively. Only the nearest atoms contribute to the σ_{iso} of the β hydrogen atoms due to the long distances to many of the other atoms.

Contributions from each atom to the σ_{iso} of the hydrogen atoms are summarized in Figure 11. The atomic contributions to the σ_{iso} values from all atoms are reported in the ESI. The 3D pictures of the MSD of the *meso* and β hydrogen atoms are reported in the ESI.

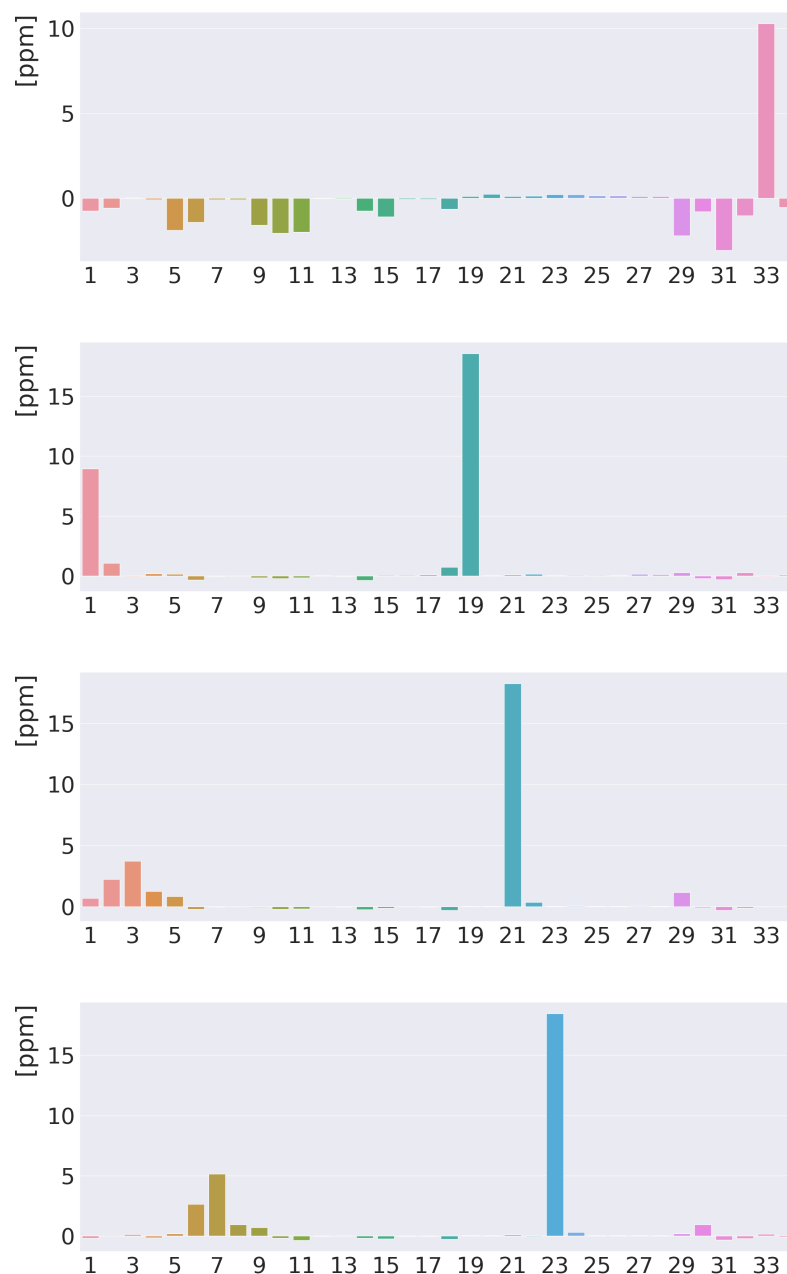


Figure 11. Atomic contributions (in ppm) to the isotropic ^1H NMR shielding constants of free-base *trans*-norcorrole. From above: the inner hydrogen, the *meso* hydrogen, the β hydrogen atoms of the pyrrole ring with an inner hydrogen, and the β hydrogen atoms of the pyrrole ring without an inner hydrogen. The atoms are numbered along the x axis in the same order as in ESI.

5. Summary and Conclusions

In the present studies on free-base *trans*-porphyrin, free-base isophlorin, and free-base *trans*-norcorrole, we have employed a method to calculate and visualize nuclear magnetic shielding densities (MSD) that was recently implemented in the GIMIC program. The MSD of the isotropic ^1H NMR shielding constants has been visualized in the molecular plane and in a plane 1 Å away from it. We also presented 3D pictures of the MSD showing the spatial origin of magnetic shielding and deshielding contributions. We have divided the molecules into atomic domains and determined atomic contributions to the isotropic ^1H NMR shielding constants by numerically integrating each domain separately.

Visualization of the MSD in the two planes shows that the main shielding contributions to the isotropic ^1H NMR shielding constant of the inner hydrogen of free-base *trans*-porphyrin originate from the diatropic ring current along the inner pathway, whereas the contributions from the outer one is smaller due to the longer distance between the inner hydrogen and the atoms along the edge of the molecule. The MSD contribution fades out as one goes away from the molecular plane. The current density in the vicinity of the studied inner hydrogen also contributes significantly to its shielding constant. The MSD of the *meso* hydrogen of free-base *trans*-porphyrin has shielding contributions from the ring current along the inner pathway and on the outside of the *meso* hydrogen. The diatropic ring current inside the *meso* hydrogen deshields its nuclear magnetic moment. Many atomic domains contribute to isotropic ^1H NMR shielding constant of the inner hydrogen, whereas the contributions to the shielding constants of the *meso* and β hydrogen atoms are dominated by contributions from the local atomic domains.

The MSD of the inner hydrogen of free-base isophlorin has large deshielding contributions from the paratropic ring current and the shielding domain appears mainly in the vicinity of the studied inner hydrogen. The contributions to MSD are stronger in the molecular plane than in the plane 1 Å away from it. The 3D picture of the MSD shows that the contribution from the inner pathway is larger than for the inner one at the remote pyrrole ring, whereas at the adjacent pyrrole rings the deshielding contribution mainly appears along the outer pathway. The *meso* hydrogen has deshielding contributions from the remote part of the paratropic ring current, whereas its contribution is shielding near the *meso* hydrogen. The current density on the outside of the *meso* hydrogen also shields its nuclear magnetic moment. Many atomic domains deshield the nuclear magnetic moment of the inner hydrogen, whereas the local contribution is shielding. The shielding contributions to the shielding constants of the *meso* and β hydrogen atoms are dominated by contributions from the atomic domains near the studied nucleus, whereas the deshielding contributions are, in comparison, very small.

Free-base *trans*-norcorrole sustains a paratropic ring current that leads to strong deshielding contributions to the MSD of the inner hydrogen. The deshielding contributions are strong in the molecular plane and in a plane 1 Å away from it. The local diatropic current density around the nitrogen moieties leads to shielding contributions that are largest at the studied inner hydrogen. The 3D picture of the MSD of the inner hydrogen shows that the molecule is dominated by deshielding contributions. Shielding contributions appear at the outer edge of the molecular ring and near the studied inner hydrogen. Integration of atomic domains shows that the largest shielding contribution appear locally, whereas the deshielding contributions from many atomic domains are almost twice as large, yielding a net deshielding contribution to the shielding constant of the inner hydrogen. The MSD of the *meso* hydrogen is dominated by local shielding contributions, whereas the remote part of the paratropic ring current deshields it. The local diatropic current density around the nitrogen moieties yields alternating shielding and deshielding contributions depending on the relative direction of the current-density flux with respect to the nucleus of the *meso* hydrogen. The shielding contributions from the atomic domains near the *meso* and β hydrogen atoms dominate their MSDs, whereas they have very few and small deshielding atomic contributions.

The present study shows the power of the present approach that can be used for determining spatial contributions to ^1H NMR magnetic shieldings. The shielding constants can be assigned to atoms by numerically integrating the MSD in atomic domains. The calculations yield the magnetically induced ring current contributions to the shielding constants of the the inner and outer hydrogen atoms of typical aromatic and anti-aromatic porphyrinoids. Here, we have focused on ^1H NMR shielding constants. However, a similar analysis can also be performed for ^{13}C NMR and ^{15}N NMR shielding constants.

Supplementary Materials: The following are available online at <https://www.mdpi.com/article/10.3390/chemistry3030072/s1>, electronic supporting information (ESI) available: the optimized molecular structures for free-base *trans*-porphyrin, free-base isophlorin and free-base *trans*-norcorrole. The atomic contributions to the isotropic ^1H NMR shielding constants and 3D pictures of the are magnetic shielding densities of the isotropic ^1H NMR shielding constants are also reported.

Author Contributions: All authors have read and agreed to the published version of the manuscript.

Funding: Funded by the Academy of Finland, the Finnish Cultural Foundation, the Swedish Cultural Foundation in Finland, and Magnus Ehrnrooth Foundation.

Institutional Review Board Statement: Not applicable.

Informed Consent Statement: Not applicable.

Data Availability Statement: Not applicable.

Acknowledgments: The work has been supported by the Academy of Finland through project number 314821, by the Finnish Cultural Foundation, the Swedish Cultural Foundation in Finland, and by Magnus Ehrnrooth Foundation. We acknowledge computational resources from CSC—IT Center for Science, Finland and the Finnish Grid and Cloud Infrastructure (persistent identifier urn:nbn:fi:research-infras-2016072533).

Conflicts of Interest: The authors declare no conflict of interest.

References

1. Lazzeretti, P.; Zanasi, R. Inconsistency of the ring-current model for the cyclopropenyl cation. *Chem. Phys. Lett.* **1981**, *80*, 533–536. [[CrossRef](#)]
2. Lazzeretti, P.; Malagoli, M.; Zanasi, R. Computational Approach to Molecular Magnetic Properties by Continuous Transformation of the Origin of the Current Density. *Chem. Phys. Lett.* **1994**, *220*, 299–304. [[CrossRef](#)]
3. Lazzeretti, P.; Malagoli, M.; Zanasi, R. *SYSMO Package*; Technical Report on Project “Sistemi Informatici e Calcolo Parallelo”; Research Report 1/67; Additional routines for the evaluation and plotting of current densities by E. Steiner, P.W. Fowler, R.W.A. Havenith, A. Soncini; University of Exeter, Exeter, UK; University of Modena; University of Salerno: Rome, Italy, 1991.
4. Monaco, G.; Summa, F.F.; Zanasi, R. Program Package for the Calculation of Origin-Independent Electron Current Density and Derived Magnetic Properties in Molecular Systems. *J. Chem. Inf. Model.* **2021**, *61*, 270–283. [[CrossRef](#)]
5. Jinger, R.K.; Fliegl, H.; Bast, R.; Dimitrova, M.; Lehtola, S.; Sundholm, D. Spatial Contributions to Nuclear Magnetic Shieldings. *J. Phys. Chem. A* **2021**, *125*, 1778–1786. [[CrossRef](#)]
6. Jusélius, J.; Sundholm, D. The aromatic pathways of porphins, chlorins and bacteriochlorins. *Phys. Chem. Chem. Phys.* **2000**, *2*, 2145–2151. [[CrossRef](#)]
7. Fliegl, H.; Pichierri, F.; Sundholm, D. Antiaromatic Character of 16 π Electron Octaethylporphyrins: Magnetically Induced Ring Currents from DFT-GIMIC Calculations. *J. Phys. Chem. A* **2015**, *119*, 2344–2350. [[CrossRef](#)]
8. Valiev, R.R.; Fliegl, H.; Sundholm, D. The aromatic character of thienopyrrole-modified 20 π -electronporphyrinoids. *Phys. Chem. Chem. Phys.* **2014**, *16*, 11010–11016. [[CrossRef](#)]
9. Pople, J.A. Molecular orbital theory of aromatic ring currents. *Mol. Phys.* **1958**, *1*, 175–180. [[CrossRef](#)]
10. McWeeny, R. Ring currents and proton magnetic resonance in aromatic molecules. *Mol. Phys.* **1958**, *1*, 311–321. [[CrossRef](#)]
11. von Ragué Schleyer, P.; Maerker, C.; Dransfeld, A.; Jiao, H.; van Eikema Hommes, N.J.R. Nucleus-Independent Chemical Shifts: A Simple and Efficient Aromaticity Probe. *J. Am. Chem. Soc.* **1996**, *118*, 6317–6318. [[CrossRef](#)]
12. Klod, S.; Kleinpeter, E. Ab initio calculation of the anisotropy effect of multiple bonds and the ring current effect of arenes-application in conformational and configurational analysis. *J. Chem. Soc. Perkin Trans.* **2001**, *2*, 1893–1898.
13. Merino, G.; Heine, T.; Seifert, G. The Induced Magnetic Field in Cyclic Molecules. *Chem. Eur. J.* **2004**, *10*, 4367–4371. [[CrossRef](#)] [[PubMed](#)]
14. Stevens, R.M.; Pitzer, R.M.; Lipscomb, W.N. Perturbed Hartree-Fock Calculations. I. Magnetic Susceptibility and Shielding in the LiH Molecule. *J. Chem. Phys.* **1963**, *38*, 550–560. [[CrossRef](#)]

15. Woodward, R.B. Totalsynthese des chlorophylls. *Angew. Chem. Int. Ed.* **1960**, *72*, 651–662. [[CrossRef](#)]
16. Reddy, B.K.; Basavarajappa, A.; Ambhore, M.D.; Anand, V.G. Isophlorinoids: The Antiaromatic Congeners of Porphyrinoids. *Chem. Rev.* **2017**, *117*, 3420–3443. [[CrossRef](#)] [[PubMed](#)]
17. Ghosh, A.; Wasbotten, I.H.; Davis, W.; Swarts, J.C. Norcorrole and Dihydronorcorrole: A Predictive Quantum Chemical Study. *Eur. J. Inorg. Chem.* **2005**, *2005*, 4479–4485. [[CrossRef](#)]
18. Bröring, M.; Köhler, S.; Kleeberg, C. Norcorrole: Observation of the Smallest Porphyrin Variant with a N₄ Core. *Angew. Chem. Int. Ed.* **2008**, *47*, 5658–5660. [[CrossRef](#)]
19. Ito, T.; Hayashi, Y.; Shimizu, S.; Shin, J.Y.; Kobayashi, N.; Shinokubo, H. Gram-Scale Synthesis of Nickel(II) Norcorrole: The Smallest Antiaromatic Porphyrinoid. *Angew. Chem. Int. Ed.* **2012**, *51*, 8542–8545. [[CrossRef](#)] [[PubMed](#)]
20. Wolinski, K.; Hinton, J.F.; Pulay, P. Efficient implementation of the gauge-independent atomic orbital method for NMR chemical shift calculations. *J. Am. Chem. Soc.* **1990**, *112*, 8251–8260. [[CrossRef](#)]
21. Helgaker, T.; Jaszuński, M.; Ruud, K. Ab initio Methods for the Calculation of NMR Shielding and Indirect Spin-Spin Coupling Constants. *Chem. Rev.* **1999**, *99*, 293–352. [[CrossRef](#)]
22. Gauss, J.; Stanton, J.F. Electron-correlated approaches for the calculation of NMR chemical shifts. *Adv. Chem. Phys.* **2002**, *123*, 355–422.
23. Facelli, J.C. Calculations of chemical shieldings: Theory and applications. *Concepts Magn. Reson. Part A* **2004**, *20A*, 42–69. [[CrossRef](#)]
24. Helgaker, T.; Coriani, S.; Jørgensen, P.; Kristensen, K.; Olsen, J.; Ruud, K. Recent Advances in Wave Function-Based Methods of Molecular-Property Calculations. *Chem. Rev.* **2012**, *112*, 543–631. [[CrossRef](#)] [[PubMed](#)]
25. Jameson, C.J.; Buckingham, A.D. Nuclear magnetic shielding density. *J. Phys. Chem.* **1979**, *83*, 3366–3371. [[CrossRef](#)]
26. Jameson, C.J.; Buckingham, A.D. Molecular electronic property density functions: The nuclear magnetic shielding density. *J. Chem. Phys.* **1980**, *73*, 5684–5692. [[CrossRef](#)]
27. Bieger, W.; Seifert, G.; Eschrig, H.; Grossmann, G. LCAO X α calculations of nuclear magnetic shielding in molecules. *Chem. Phys. Lett.* **1985**, *115*, 275–280. [[CrossRef](#)]
28. Mohr, P.J.; Newell, D.B.; Taylor, B.N. CODATA Recommended Values of the Fundamental Physical Constants: 2014. *J. Phys. Chem. Ref. Data* **2016**, *45*, 043102. [[CrossRef](#)]
29. Jusélius, J.; Sundholm, D.; Gauss, J. Calculation of Current Densities using Gauge-Including Atomic Orbitals. *J. Chem. Phys.* **2004**, *121*, 3952–3963. [[CrossRef](#)] [[PubMed](#)]
30. Taubert, S.; Sundholm, D.; Jusélius, J. Calculation of spin-current densities using gauge-including atomic orbitals. *J. Chem. Phys.* **2011**, *134*, 054123. [[CrossRef](#)]
31. Fliegl, H.; Taubert, S.; Lehtonen, O.; Sundholm, D. The gauge including magnetically induced current method. *Phys. Chem. Chem. Phys.* **2011**, *13*, 20500–20518. [[CrossRef](#)]
32. Sundholm, D.; Fliegl, H.; Berger, R.J.F. Calculations of magnetically induced current densities: Theory and applications. *WIREs Comput. Mol. Sci.* **2016**, *6*, 639–678. [[CrossRef](#)]
33. Dimitrova, M.; Sundholm, D. Current density, current-density pathways and molecular aromaticity. In *Aromaticity: Modern Computational Methods and Applications*; Fernández López I., Ed.; Elsevier: Amsterdam, The Netherlands, 2021; Chapter 5, pp. 155–194.
34. GIMIC, Version 2.0, a Current Density Program. December 2020. Available online: <https://github.com/qmcurrents/gimic> (accessed on 3 September 2021).
35. Sambe, H. Properties of induced electron current density of a molecule under a static uniform magnetic field. *J. Chem. Phys.* **1973**, *59*, 555. [[CrossRef](#)]
36. Lazzeretti, P. Current density tensors. *J. Chem. Phys.* **2018**, *148*, 134109. [[CrossRef](#)] [[PubMed](#)]
37. Lazzeretti, P. Ring currents. *Prog. Nucl. Magn. Reson. Spectrosc.* **2000**, *36*, 1–88. [[CrossRef](#)]
38. Pelloni, S.; Lazzeretti, P. On the existence of a natural common gauge-origin for the calculation of magnetic properties of atoms and molecules via gaugeless basis sets. *J. Chem. Phys.* **2012**, *136*, 164110. [[CrossRef](#)] [[PubMed](#)]
39. Lazzeretti, P.; Malagoli, M.; Zanasi, R. Electronic Current-Density Induced by Nuclear Magnetic Dipoles. *J. Mol. Struct.: THEOCHEM* **1994**, *119*, 299–304. [[CrossRef](#)]
40. Komorovsky, S.; Jakubowska, K.; Świder, P.; Repisky, M.; Jaszuński, M. NMR Spin-Spin Coupling Constants Derived from Relativistic Four-Component DFT Theory-Analysis and Visualization. *J. Phys. Chem. A* **2020**, *124*, 5157–5169. [[CrossRef](#)]
41. Lehtola, S.; Dimitrova, M.; Fliegl, H.; Sundholm, D. Benchmarking Magnetizabilities with Recent Density Functionals. *J. Chem. Theory Comput.* **2021**, *17*, 1457–1468. [[CrossRef](#)]
42. Keith, T.A.; Bader, R.F.W. Calculation of Magnetic Response Properties Using a Continuous Set of Gauge Transformations. *Chem. Phys. Lett.* **1993**, *210*, 223–231. [[CrossRef](#)]
43. Steiner, E.; Fowler, P.W. Patterns of Ring Currents in Conjugated Molecules: A Few-Electron Model Based on Orbital Contributions. *J. Phys. Chem. A* **2001**, *105*, 9553–9562. [[CrossRef](#)]
44. Soncini, A.; Fowler, P.; Lazzeretti, P.; Zanasi, R. Ring-current signatures in shielding-density maps. *Chem. Phys. Lett.* **2005**, *401*, 164–169. [[CrossRef](#)]
45. Pelloni, S.; Ligabue, A.; Lazzeretti, P. Ring-Current Models from the Differential Biot-Savart Law. *Org. Lett.* **2004**, *6*, 4451–4454. [[CrossRef](#)] [[PubMed](#)]

46. Ferraro, M.; Lazzeretti, P.; Viglione, R.; Zanasi, R. Understanding proton magnetic shielding in the benzene molecule. *Chem. Phys. Lett.* **2004**, *390*, 268–271. [CrossRef]
47. Steiner, E.; Fowler, P.W. On the orbital analysis of magnetic properties. *Phys. Chem. Chem. Phys.* **2004**, *6*, 261–272. [CrossRef]
48. Ferraro, M.B.; Faglioni, F.; Ligabue, A.; Pelloni, S.; Lazzeretti, P. Ring current effects on nuclear magnetic shielding of carbon in the benzene molecule. *Magn. Res. Chem.* **2005**, *43*, 316–320. [CrossRef]
49. Acke, G.; Van Damme, S.; Havenith, R.W.A.; Bultinck, P. Interpreting the behavior of the NICS_{zz} by resolving in orbitals, sign, and positions. *J. Comp. Chem.* **2018**, *39*, 511–519. [CrossRef]
50. Acke, G.; Van Damme, S.; Havenith, R.W.A.; Bultinck, P. Quantifying the conceptual problems associated with the isotropic NICS through analyses of its underlying density. *Phys. Chem. Chem. Phys.* **2019**, *21*, 3145–3153. [CrossRef]
51. Balasubramani, S.G.; Chen, G.P.; Coriani, S.; Diedenhofen, M.; Frank, M.S.; Franzke, Y.J.; Furche, F.; Grotjahn, R.; Harding, M.E.; Hättig, C.; et al. TURBOMOLE: Modular program suite for ab initio quantum-chemical and condensed-matter simulations. *J. Chem. Phys.* **2020**, *152*, 184107. [CrossRef]
52. Becke, A.D. Density-functional thermochemistry. III. The role of exact exchange. *J. Chem. Phys.* **1993**, *98*, 5648–5652. [CrossRef]
53. Lee, C.; Yang, W.; Parr, R.G. Development of the Colle-Salvetti correlation-energy formula into a functional of the electron density. *Phys. Rev. B* **1988**, *37*, 785–789. [CrossRef]
54. Stephens, P.J.; Devlin, F.J.; Chabalowski, C.F.; Frisch, M.J. Ab Initio Calculation of Vibrational Absorption and Circular Dichroism Spectra Using Density Functional Force Fields. *J. Phys. Chem.* **1994**, *98*, 11623–11627. [CrossRef]
55. Weigend, F.; Ahlrichs, R. Balanced basis sets of split valence, triple zeta valence and quadruple zeta valence quality for H to Rn: Design and assessment of accuracy. *Phys. Chem. Chem. Phys.* **2005**, *7*, 3297–3305. [CrossRef] [PubMed]
56. Eichkorn, K.; Weigend, F.; Treutler, O.; Ahlrichs, R. Auxiliary basis sets for main row atoms and transition metals and their use to approximate Coulomb potentials. *Theor. Chim. Acta* **1997**, *97*, 119–124. [CrossRef]
57. Treutler, O.; Ahlrichs, R. Efficient molecular numerical integration schemes. *J. Chem. Phys.* **1995**, *102*, 346–354. [CrossRef]
58. Becke, A.D. Density-functional exchange-energy approximation with correct asymptotic behavior. *Phys. Rev. A* **1988**, *38*, 3098–3100. [CrossRef]
59. Becke, A.D. A new mixing of Hartree-Fock and local density-functional theories. *J. Chem. Phys.* **1993**, *98*, 1372–1377. [CrossRef]
60. Ditchfield, R. Self-Consistent Perturbation-Theory Of Diamagnetism 1. Gauge-Invariant LCAO Method For NMR Chemical-Shifts. *Mol. Phys.* **1974**, *27*, 789–807. [CrossRef]
61. Kollwitz, M.; Häser, M.; Gauss, J. Non-Abelian point group symmetry in direct second-order many-body perturbation theory calculations of NMR chemical shifts. *J. Chem. Phys.* **1998**, *108*, 8295–8301. [CrossRef]
62. Reiter, K.; Mack, F.; Weigend, F. Calculation of Magnetic Shielding Constants with meta-GGA Functionals Employing the Multipole-Accelerated Resolution of the Identity: Implementation and Assessment of Accuracy and Efficiency. *J. Chem. Theory Comput.* **2018**, *14*, 191–197. [CrossRef]
63. Jensen, F. Unifying General and Segmented Contracted Basis Sets. Segmented Polarization Consistent Basis Sets. *J. Chem. Theory Comput.* **2014**, *10*, 1074–1085. [CrossRef]
64. Pritchard, B.P.; Altarawy, D.; Didier, B.; Gibbs, T.D.; Windus, T.L. A New Basis Set Exchange: An Open, Up-to-date Resource for the Molecular Sciences Community. *J. Chem. Inf. Model.* **2019**, *59*, 4814–4820. [CrossRef] [PubMed]
65. Feller, D. The role of databases in support of computational chemistry calculations. *J. Comput. Chem.* **1996**, *17*, 1571–1586. [CrossRef]
66. Schuchardt, K.L.; Didier, B.T.; Elsethagen, T.; Sun, L.; Gurumoorthi, V.; Chase, J.; Li, J.; Windus, T.L. Basis Set Exchange: A Community Database for Computational Sciences. *J. Chem. Inf. Model.* **2007**, *47*, 1045–1052. [CrossRef]
67. Pecul, M.; Ruud, K. The ab initio calculation of optical rotation and electronic circular dichroism. *Adv. Quantum Chem.* **2005**, *50*, 185–212.
68. Fliegl, H.; Sundholm, D.; Taubert, S.; Jusélius, J.; Klopper, W. Magnetically Induced Current Densities in Aromatic, Antiaromatic, Homoaromatic, and Nonaromatic Hydrocarbons. *J. Phys. Chem. A* **2009**, *113*, 8668–8676. [CrossRef] [PubMed]
69. Bast, R., April 2020. Numgrid v1.1.2: Numerical Integration Grid for Molecules. Available online: <https://zenodo.org/record/4815722#.YThHNty-s2w> (accessed on 3 September 2021).
70. Becke, A.D. A multicenter numerical integration scheme for polyatomic molecules. *J. Chem. Phys.* **1988**, *88*, 2547–2553. [CrossRef]
71. Lebedev, V.I. A quadrature formula for the sphere of 59th algebraic order of accuracy. *Russ. Acad. Sci. Dokl. Math.* **1995**, *50*, 283–286.
72. Lindh, R.; Malmqvist, P.Å.; Gagliardi, L. Molecular integrals by numerical quadrature. I. Radial integration. *Theor. Chem. Acc.* **2001**, *106*, 178–187. [CrossRef]
73. Fliegl, H.; Sundholm, D. Aromatic Pathways of Porphins, Chlorins and Bacteriochlorins. *J. Org. Chem.* **2012**, *77*, 3408–3414. [CrossRef]
74. Nozawa, R.; Kim, J.; Oh, J.; Lamping, A.; Wang, Y.; Shimizu, S.; Hisaki, I.; Kowalczyk, T.; Fliegl, H.; Kim, D.; Shinokubo, H. Three-dimensional aromaticity in an antiaromatic cyclophane. *Nat. Commun.* **2019**, *10*, 3576. [CrossRef]
75. Sundholm, D.; Fliegl, H. Aromatic Pathways in Porphyrinoids by Magnetically Induced Ring Currents. In *Handbook of Porphyrin Science*; Kadish, K.M.; Smith, K.M.; Guillard, R., Eds.; World Scientific: Singapore, 2021; Volume 46, in press.
76. Kawashima, H.; Ukai, S.; Nozawa, R.; Fukui, N.; Fitzsimmons, G.; Kowalczyk, T.; Fliegl, H.; Shinokubo, H. Determinant Factors of Three-Dimensional Aromaticity in Antiaromatic Cyclophanes. *J. Am. Chem. Soc.* **2021**, *143*, 10676–10685. [CrossRef] [PubMed]